

Review on Property of Ca-Hexa Ferrites in Material Development

Jay Singh Sagar¹, A. P. Bhat², K. G. Rewatkar³, D. K. Sahu⁴

¹Department of Physics, Institute of Basic science Bundelkhand university, Jhansi-284128, India

²Department of Electronics, Aolachand Mahavidyalaya Yavtmal-445001, India

³Department of Physics, Dr. Ambedkar College, Deekashabhoomi Nagpur-440010, India

⁴Department of Physics, R.S. Government P.G. College, Lalaitpur-204403, India

Corresponding Author: phdjaysinghsagar@gmail.com, anup_b5@yahoo.com

Abstract

The requirement for present-day magnetics in the new time of innovation Researchers was persuaded by materials to do the investigation on hexagonal Because of their wide uses as attractive materials, ferrites principally. Ferrites have gotten basic for business and innovation the same. Uses. Uses. Their executions depend on extremely basic highlights. Viz., Magnetization of immersion, high electrical resistivity, low electrical resistivity, Chemical Stability, and Losses. The nanosize end, uncommon and exceptional It has procured mechanically interesting resources. Nanoparticles, on the other hand, maybe changed with different forms of nano-particles Structures by various methods of synthesis and substitutions to Boost their attributes. The most popular magnetic applications are Recording, products for data storage, ferrofluids, and distribution of medicines.

The combustion of the solution and hydrothermal synthesis results from the elite. Structural characteristics are described as the compound and its structural, electrical, and magnetic properties are Reviewed based on the synthesis process.

Keywords: *ferrite, substituted ferrites, stability, magnetic property, electrical properties, Curi temperature*

1. Introduction

Ferrite materials are attractive materials that all the while having ferromagnetic properties and high protection from electrical current [1]. Iron oxide and metal oxides are the primary parts of the ferrites. High electrical resistivity, low dielectric misfortune, high charge, and immersion penetrability, just as gentle permittivity are additionally protected and have attractive oxides. Ferrites are semiconducting attractive oxide items that are of extraordinary specialized significance because of their fascinating electrical and attractive properties. They are utilized in high thickness attractive capacity media, perpetual magnets, transducers, PC and microwave advancements, transformer centers, receiving wire bars, memory chips, etc.. They have three unmistakable underlying balances: grants, hexagonal, and cubic,

characterized by the size and charge of the metal particles that balance the charge and relative centralizations of the oxygen particles[2, 3].

In most of the ferrite items, doping or substituent assume a significant part in deciding the variety of the actual properties, attractive and electrical vehicle properties. The replacement can be isolated into the accompanying sorts: the immediate supplanting of Fe^{+3} with the substituent particle on the tetrahedral (A) or octahedral (B) sublattice, bringing about the reallocation of Fe^{+3} particles among A-and B-sublattices, bringing about the adjustment in the ferromagnetic turn structure. The degree of the iron reallocation relies upon the specific presence of the particle replacement [[4,5]].

In light of their capacity to be polarized and demagnetized, ferrites are partitioned into two sorts: delicate and strong. It is anything but difficult to polarize and demagnetize delicate ferrite materials, so they are utilized for electromagnets, while perpetual magnets [1, 6] utilize hard ferrite materials.

Ferrites are profoundly touchy to the readiness cycle, the state of sintering, the number of constituent metal oxides, and the subbed dopants or components. The underlying and attractive properties of ferrites are discovered to be touchy to their organization and microstructure, contingent upon preparing conditions. Different types of amalgamation strategies have been created to get ready unadulterated

Furthermore, doped ferrite materials, for example, a strong state, sol-gel, aqueous, auto-burning, and so on [2,3]. Among the accessible strategies for amalgamation, the Sol-gel procedure has been broadly utilized in the readiness of ferrite materials since it offers significant focal points, for example, the better blending of the beginning materials and magnificent substance homogeneity in the last product[4-6].

These materials have low electrical conductivity contrasted and other attractive materials and are accordingly broadly utilized at microwave frequencies. M-ferrites are semiconductors with their conductivity lying somewhere in the range of 10^2 and $10^{11} \text{ Ohm}^{-1} \text{ cm}^{-1}$. The reason for the conductivity is the presence of Fe^{2+} and the metal M^{3+} particles. $\text{Fe}^{3+} + e - \text{Fe}^{2+}$ electron jumping is given by iron particles and M^{3+} particles give $\text{M}^{2+} + \text{h}^+ + \text{M}^{3+}$ [14] opening bouncing. The development is explained by a bouncing instrument wherein the charge transporters hop from one ionic site to another[5-7]. Fe^{2+} applies to n-type lead and M^{3+} to p-type direct. Because of the versatility around the additional electron's precious stone cross-section or the positive hole[8], conductivity exists.

There has been a think productively extent of interest in hexagonal ferrites since its revelation during the 1950s, which is as yet developing today. In 2011 and 2019, a record number of hexaferrite papers have been delivered. In the most recent decade, there has been a blast of interest in hexaferrite in more whimsical applications, just as in their particular attractive properties, use as attractive chronicle and information stockpiling materials, and consistent comprehension of their MW properties. Specifically, this applies to MW/GHz electronic segments and EM safeguards (RAM) and engineered structures.

Over the years, magnetoplumbite ferrite (M-Type) has drawn more interest from many researchers because of its various categories of applications over a large frequency spectrum, low cost, and high performance[1]. A new class of ferrites with a permanent magnetic property, known as hexagonal ferrites, with the formula $MFe_{12}O_{19}$, where M is the divalent metal cation and can be substituted by an equivalent cation or its combination[2]. Alkaline metals are either barium, strontium, calcium, or lead. One of the most common hard magnetic materials with the general formula $CaMFe_{12}O_{19}$ and mixed ferrites is $Ca_xM_{1-x}Fe_{12-x}O_{19}$, where M= Al, Sr, Cr, is commonly used for the above-mentioned uses. The M-type is very beneficial for microwave applications [3]. The magnetic and electrical properties of the hexagonal ferrites will be changed by doping of different cations at M (Ca, Sr, Ba, Pb). Numerous cations and their mixes have been substituted with M-type hexagonal ferrites[4-6] by a few scientists.

1.1.1 Arrangement of the ferrites

There are firmly associated, very unpredictable gem structures of all hexagonal ferrites[18], which can be spoken to unexpectedly. At the essential level, the three ferrites intensify S (spinel, $MeFe_2O_4$), M ($BaFe_{12}O_{19}$), and Y all can be viewed as atomic mixes ($Ba_{2-x}Me_xFe_{12}O_{22}$). $M^{+2}S$, X-ferrite ($Ba_2Me_2Fe_{28}O_{46}$)= $W+M=2M+2S$, Z-ferrite ($Ba^3Me^2Fe_{24}O_{41}$)= $M+Y$, and U-ferrite ($Ba^4Me^2Fe_{36}O_{60}$)= $Z+M=2M+Y$ can be considered as W-ferrite, $BaMe^2Fe_{16}O_{27}$. Y. Sudhakar et al.[2-5] announced HRTEM pictures of the stacking of these layers. The other bigger hexagonal ferrites are created correspondingly.

The Ba^{2+} particle, similar to the O^{2-} particle, is enormous, and perhaps in the oxygen cross-section, an oxygen ion is regularly supplanted by barium. As the barium particle is fundamentally more modest than the oxygen particle, the cross-section in its nearby region is slanted by this. The barium particle might be supplanted by another divalent metal if there are sufficient sizes, for example, strontium or lead, to protect the structure without an excessive amount of twisting. In Fe^{3+} and Me^{2+} , the three-sided bipyramidal site is a lot more modest particles and is consolidated in interstices between oxygen positions. The divalent and trivalent particles in octahedral and tetrahedral areas in the structure are present with oxygen, just as in hexaferrite containing the R block[8-9].

Four Miller Indices to portray a hexagonal precious stone. The fundamental hub is along the length of the gem in the (0001) heading, and the three different tomahawks are at points of 120° to one another along the hexagonal polyhedron's basal (0001) plane. The c-axis is known as the vital axis and the cross-section boundary is its thickness. The three tomahawks of the hexagonal plane are largely equivalent in the ferrites, thus just a single extra boundary is expected to characterize the ordinary hexagonal precious stone, the length of the plane on one side. To give the components of the gem, just two cross-section boundaries, c and a are subsequently required.

Table 1 Descriptions of the molecular units of hexagonal ferrites[1].

Ferrite	Molecular formula	Molecular units	Spinel plates and hexagonal layers	Hexaferrite blocks
S	CoFe_2O_4	S	S_1	1/2 S
M	$\text{BaFe}_{12}\text{O}_{19}$	M	$M_5 = B_1S_4$	SR
W	$\text{BaCo}_2\text{Fe}_{16}\text{O}_{27}$	M + 2S	$W_7 = M_5S_2 = B_1S_6$	SSR
X	$\text{Ba}_2\text{Co}_2\text{Fe}_{28}\text{O}_{46}$	2M + 2S	$X_{12} = M_5S_2 M_5 = B_1S_4B_1S_6$	SRS SR
Y	$\text{Ba}_2\text{Co}_2\text{Fe}_{12}\text{O}_{22}$	Y	$Y_6 = B_2S_4$	SI
Z	$\text{Ba}_3\text{Co}_2\text{Fe}_{24}\text{O}_{41}$	Y+M	$Z_{11} = Y_6M_5 = B_2S_4B_1S_4$	STSR
U	$\text{Ba}_4\text{Co}_2\text{Fe}_{36}\text{O}_{60}$	Y+2 M	$U_{16} = M_5Y_6 M_5 = B_1S_4B_2S_4B_1S_4$	SRS RST

1.1.2 The S, R, and T Blocks

The S block comprises two units of spinel and hence has the recipe of the $\text{Me}^2\text{Fe}_4\text{O}_8$ unit, where Me is equivalent to the unit of S_2 , where Me is a divalent metal particle. Thus, every S block comprises four oxygen atoms in two layers with three metal particles in each layer, 4 octahedral locales with six oxygen anions encompassing the cation, and two tetrahedral destinations with four oxygen atoms encompassing the cation.

The R block comprises of 3-hexagonally stuffed layers of 4-oxygen atoms each, yet one of the oxygen molecules is at the center layer is supplanted with a comparably measured barium particle to give the unit recipe $\text{BaFe}_6\text{O}_{11}$. This is like the M_5 unit, with the top and the base layers eliminated. The single barium particle in the square makes an imbalance in a portion of the cation locales, bringing about five octahedral destinations, no tetrahedral destinations, as the cumbersome barium molecule is driven into octahedral destinations, and a five-arrange three-sided bipyramidal site where five oxygen anions encompass the cation, a unique position discovered distinctly in the R block[1,3,5].

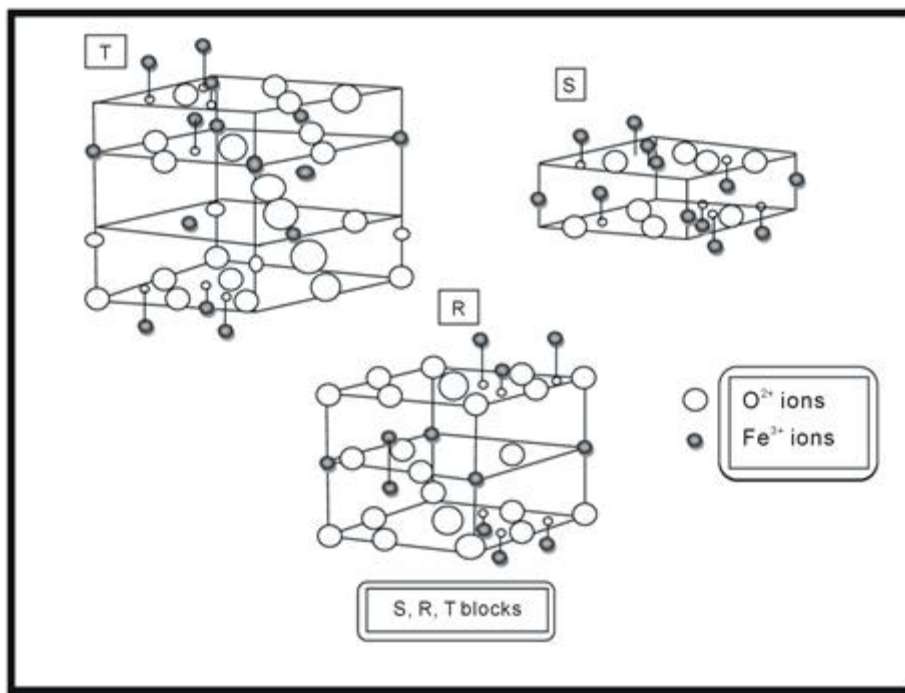


Figure 1: S-R-T-Block game plan of Fe-O-M Molecules in Hexa ferrites

The T block is contained four oxygen layers, with a barium bit displacing an oxygen particle in the point of convergence of two layers, to give the $Ba_2Fe_8O_{14}$ condition. Again this is the Y6 unit with the top and base layers disposed of. Since two far-reaching barium particles reverse each other in adjoining layers, both the barium and the cations that would have been in the five-encourage positions are moved conversely. This reduces the five-mastermind three-sided bipyramidal districts to four-encourage tetrahedral objections, achieving two tetrahedral regions and six octahedral regions.

The authentic unit cells of most hexagonal ferrites involve results of sub-nuclear ferrites, two ferrite sub-nuclear units for M, W, and Z, and three ferrite sub-nuclear units for X and Y, yet a solitary ferrite sub-nuclear unit for U. As a result of the dynamical nature and tremendous size of the unit cells, particular jewels of these ferrites can be outstandingly enormous[1,5].

1.1.3 The M structure

The sub-atomic unit of M ferrite comprises of one S and R block, with a cover of layers stuffed hexagonally and cubically. The basal plane of the 3+ molecule is along these lines a mirror plane and the two S hinders above and underneath the R block are 180°C pivots around the c-hub of one another. Hence, the unit cell requires two atomic M units, giving the unit cell equation S-R-S-R, where the angle is 180 degrees around the c-axis. the c-axis parameter, the CaM cross-section boundaries are 22.17Å and for the basal plane width, 5.89Å, and this a-boundary is a steady hexagonal ferrite boundary. The tallness to width proportion is 3.94 Å, so M has an expansive translucent anisotropy, the other hexagonal ferrites turns out to be much higher.

Because of the lower size of the Sr^{2+} particle, SrM has more modest section constants, giving the boundaries $c = 23.03 \text{ \AA}$ and $a = 5.86 \text{ \AA}$. It has a similar structure as BaM[14]. The Pb^{2+} particle is likewise more modest than Ba^{2+} , with $c = 23.02 \text{ \AA}$, $a = 5.88 \text{ \AA}$ [1,3] being the cross-section boundaries for PbM.

1.1.4 Ferrite electric conductivity

While hexagonal ferrites are acceptable electrical resistors, even in little amounts, the obstruction diminishes altogether when the bivalent ferrous particle (Fe^{2+}) is appended to the ferric particle (Fe^{3+}), as an exceptionally quick electron exchange ('bouncing') can happen, producing a current[35]. This is the reason magnetite is quite a solid oxide conduit for power. Two elective pathways of conduction are accessible, n-type electron conduction and p-type opening conduction. If one cation is supplanted by another, that needs a lower valency level in high-obstruction materials, at that point, p-type conduction happens when a higher valence is chosen by the cation, at that point n-type results.

Abundance iron (or high-temperature sintering oxygen insufficiency) in ferrites encourages Fe^{2+} arrangement and results in n-type conduction, yet iron inadequacy adds to p-type conduction, in ferrites[36]. If the material is to have such electrical uses, a bounty of iron may likewise be evaded. Shockingly, the extent of Fe^{2+} in ferrite is additionally expanded because of the high sintering temperatures needed to advance a thick item, even though the option of manganese or cobalt in sums as low as 0.02 percent decreases the obstruction by a few sets of magnitude [3-7].

Low opposition grains are regularly isolated by profoundly resistive grain limits in polycrystalline earthenware ferrites, making an interfacial polarization that could prompt conductivity that would be decreased in bigger grained ferrites. In cobalt-containing ferrites, the $\text{Fe}^{3+} - \text{Fe}^{2+}$ design has been declared to be decreased by the $\text{Fe}^{2+} + \text{Ca}^{3+} \text{Fe}^{3+} + \text{Ca}^{2+}$ response, and other stable multivalent particles, for example, Al-Mn will have a comparable impact. Al Mn^{3+} is thought to expand resistivity to a more noteworthy degree than Ca^{3+} because it shapes a stable confined pair of $\text{Al-Mn}^{3+}\text{Fe}^{2+}$, keeping electrons from leaving Fe^{2+} for other ferric ions[8].

The S block comprises of two spinel units and subsequently has the $\text{Me}_2\text{Fe}_4\text{O}_8$ unit equation, where Me is equivalent to the S2 unit, where Me is a divalent metal particle. Therefore, every S block comprises two layers of four oxygen particles with three metal molecules in each layer, four octahedral locales encompassing the cation with six oxygen anions, and two tetrahedral destinations encompassing the cation with four oxygen anions.

The R block comprises three hexagonally pressed layers of four oxygen particles each, however, to give the unit recipe $\text{BaFe}_6\text{O}_{11}$, one of the oxygen iotas in the center layer is subbed by a correspondingly measured barium molecule. With the top and the base layers eliminated, this is like the M5 unit. In a portion of the cation destinations, the single barium particle in the square makes a deviation, bringing about five octahedral locales, no tetrahedral destinations, as the massive barium iota is driven into octahedral destinations, and a five-

facilitate bipyramidal three-sided site where the cation is encircled by five oxygen anions, an extraordinary position discovered distinctly in the R block[9].

1.2 Synthesis methods

The arrangement of hexagonal ferrites is a very confounded cycle, and the components engaged with an affidavit of dopant at the explicit site are not completely perceived, regardless of having been read by a few scientists for more than 50 years[1, 5-8].

Table 2: temperature-subordinate blend and bi-items as major and minor

Temp	Major products	Minor products	Fuel
500 °C	α -Fe ₂ O ₃ , Ca ₃ O ₄ , CaO		Urea, Glycine, Citic acid
600 °C	α -Fe ₂ O ₃ , Ca ₃ O ₄ , CaO	CaFe ₂ O ₄ , CaFe ₂ O ₄	Urea/ glycine, citic acid
700 °C	α -Fe ₂ O ₃ , CaFe ₂ O ₄ , CaFe ₂ O ₄	CaM, CaO	Urea/ glycine
800 °C	CaM, CaFe ₂ O ₄	α -Fe ₂ O ₃ , CaFe ₂ O ₄	Urea/ glycine
900 °C	CaM, Y	CaFe ₂ O ₄ , CaFe ₂ O ₄	Urea/ glycine
1000 °C	BaM, Y	CaFe ₂ O ₄ , CaFe ₂ O ₄	Urea/ glycine
1100 °C	Y, BaM	CaFe ₂ O ₄	Urea/ glycine
1200 °C	Z, Y, BaM	W	Urea/ glycine

As can be seen, all the different hexagonal stages cover and, except for the M ferrites, they all require high temperatures of at any rate 1000°C to turn into the primary stage. This makes it amazingly difficult to get single-stage examples of a portion of these ferrites, and in light of the high temperatures required, their molecule size will in general be huge. A misrepresented rising example is seen at temperatures over 1200°C in which a few particles extend to a far more prominent degree and at a higher movement than their neighbors, even in a solitary stage material. This morphology is alluded to as broken grain development (DGG) and individual hexagonal grains with a measurement of up to 10nm, containing huge molecule distance across spreads of up to a few tens or even many lm, can be created[11].

1.2.1 Ceramics of standard

To accomplish the ideal stage, standard fired strategies used to set up the hexagonal ferrites incorporate heating a combination of oxide and barium carbonate powders. To make a better material, the earthenware item at that point typically must be processed and powdered and afterward sintered to expand thickness. The necessary high temperatures and long terminating times for the most part bring about a coarse grain item, with M-ferrites averaging grain sizes somewhere in the range of 1 and 10 nm. Be that as it may, crystallization happens at lower temperatures, bringing about more modest particles and lower sintering temperatures, if the beginning materials are blended personally at the nuclear or ionic stage preceding response, and the completely densified material can in this manner be created in one stage. This can be cultivated by mechanochemical processing of high energy, by and large in a planetary ball plant of high energy. The idea of the hexaferrite being gathered by topotactic responses from

prior translucent development blocks makes them ideal for this kind of combination, particularly the more intricate mixes.

1.2.1 Co-precipitation

For the creation of ferrites[1,12], substance co-precipitation of salts with a base bringing about an encourage containing all the segments blended at an ionic stage was utilized. It has additionally been discovered that an iron-lacking non-stoichiometric combination must be utilized rather than the right proportion of 12[12] with a Fe: Ca proportion of 10:11 for CaM, for example. To give unadulterated M[53] from co-hastens, SrM requires an even lower Fe: Ca proportion of under 9:7. CaM can be shaped with a submicron grain size at temperatures somewhere in the range of 750 and 900°C utilizing this cycle, and the item thickness can be expanded on the off chance that it is washed by rotator when contrasted with decantation[5-4].

A wet compound technique was shaped to improve homogeneity, in which a moisture arrangement of salts with a solid base was hastened. the subsequent hydroxide was oxidized by foaming air to create a homogeneous fine-grained ferrite substance [13]. In later work, NaOH is co-accelerated at pH9-14 with a non-stoichiometric arrangement of iron(II) and calcium salts, and the subsequent hydroxides are oxidized and afterward washed at pH-7 with hydrogen peroxide (H₂O₂). At an extremely low temperature of 400-600°C and producing a grain size of below 100 nm[56], it at that point warms the dried hydroxides and produces unadulterated BaM.

1.2.3 Method of Salt-dissolve

In this cycle, NaOH, Na₂CO₃, or NaHCO₃ are co-accelerated with an answer of metal chlorides, and afterward, NaCl and additionally KCl salts are added to the combination, which is then dried near to 600-1100°C to give a cooling combination of ferrite and soluble metal salts[5-8]. The underlying methodology, which brought about an unrivaled item with simply a blend of standard clay pre-cursors, was less exceptional. It is anything but difficult to separate sodium and potassium salts from ferrite by washing with water or weaken acids, yet there is some basic metal pollution of the ferrite content.

In a non-stoichiometric blend with Fe, CaM with great magnetic properties was created by this strategy: by changing the arrangements of the fluxing segments, the Ca proportion of 10:11, and the submicron grain size and magnetic properties can fluctuate Soften transition precipitation is a variety of this technique where less fluxing material is included quite a route that there are just microregions of marginally dissolved salt wherein crystallization happens as opposed to making a genuine arrangement of the fluid stage. The unadulterated ferrite was framed at a lower temperature and with a grain size of 33% of the size at under 100 nm when the dissolve motion was radio-thermally warmed by an electron shaft rather than ordinary warm heating[3].

1.2.4 Gel-sol

The sol-gel technique consolidates antecedent particles that on the colloidal scale might be inorganic or Metallo-natural, this blending is safeguarded when the material is dense to form a gel, and fine-grained polycrystalline ferrites with a little size appropriation were set up by this strategy. The sol must be essential if it contains hastens because this compound is just steady at a high pH and consequently, corrosive absorption and peptization can't comprise such a sol. Glycine, a natural organizing specialist, for example, ethylene glycol and urea, is additionally added to the sun oriented hydroxide arrangement, which gives a gel structure after vanishing of water. M ferrite with a grain size of only 60 nm at 900°C/1 h [6-8]. Unadulterated M with no α -Fe₂O₃ a subsequent move yielded,

Various hexagonal ferrites are added from stoichiometric forerunners, adding aluminum, strontium, and cobalt salts to a corrosive peptized iron(III)hydroxide (FeOOH) sol, fluid microwave-helped auto combusted sol-gel course was delivered by K. G. Rewatkar et al.

Halide and nitrate salts, soles settled by halide –nitrate combination, have likewise been examined. For resulting handling, for example, turn covering, thick film, and fiber creation, the strength of a sol, and how thought it very well may be delivered, is significant. With dissolvable molecule sizes of 4.7 and 6.8nm, individually. the low polydispersity, both halide-and nitrate-settled undoped iron(III) soles were entirely steady, yet halide counterion-balanced outsoles were more steady and up to 35.5 percent, Fe³⁺ could be concentrated with just water as a dissolvable, while the most extreme nitrate-based iron(III) sol fixation was 23.5 % Fe³⁺[7].

In reality, given a lot bigger 'tail' of up to 31.5nm contrasted with 20 nm for the halide sol[77] for the normal volume of the nitrate sol, the furthest reaches of sol molecule size and few bigger particles are critical to making the sol destabilize and accelerate when consolidated.

With a monodisperse typical age sol particle size of only 8nm, the stoichiometric SrM trailblazer delivered utilizing a NO⁻³ based sol was altogether consistent, which could be ideal up to 17 % Fe³⁺, while the BaM precursor sol created utilizing nitrates was polydisperse and essentially less consistent with a mean sol atom size of 54 nm and a most extreme limitation of 282nm[12-13]. It was in like manner say that the development of a chelating ligand of the crown ether to the sol fundamentally improved the steadfastness of all sols containing barium. Completely consistent stoichiometric sol precursors were made from all the recently referenced hexagonal ferrites using a sans nitrate sol-gel structure with the extension of cobalt halide salt, with ordinary sol atom sizes under 10 nm in all cases, which were changed over to hexaferrite in a single stage between 700°C (SrM) and 1200°C (Co₂W and Co₂Z) [3,14].

A sol-gel strategy that evades both coprecipitation and Metallo-natural mixes is the stearic corrosive gel method. In liquid stearic corrosive, a stoichiometric salt blend is disintegrated and warmed at 80-120°C/2 h to frame a straightforward sol, shaping a homogeneous gel intermixed at the nuclear level after cooling. This outcomes in the arrangement of nanocrystalline materials at low temperatures after a natural part have been combusted at 450°C[10-13].

1.2.6 Hydrothermal synthesis

An answer of metal salts and a base is autoclaved under tension in the aqueous blend to create the part. The outcome is frequently a blended stage containing unreacted forerunners and at times α -Fe₂O₃, which is removed through weakening HCl washing. The aftereffects of the utilization of NaOH, KOH, (C₂H₅)₄NOH, and NH₄OH as bases of CaM combination were broken down by Ataie et al. also, found that NaOH and KOH gave micron-sized CaM platelets at 220°C/5 h[8-7]. CaM was likewise delivered at 332°C/5 h via autoclaving combinations of metal nitrates and NaOH, which was then tempered at 900 °C to flexibly the unadulterated translucent item. The unadulterated period of BaM can likewise be produced using stoichiometric mixtures[88], however, this is a co-precipitation strategy also. The aqueous union was likewise utilized at low temperatures to deliver more intricate hexaferrite, for example, Fe₂Y, however, it disintegrated to CaM and CaFe₂O₄ over 900°C[9,2].

1.2.8 The Method for Combustion

The arrangement of salts, alkali, and citrus extract at pH-7 has vanished into dryness on a hot plate in a variation of the citrate cycle, so, all in all, a self-engendering decay occurred. As the citrus extract polymerized, a frothy mass expands and lighted and created CO₂ in a fierce exothermic response that spread over the whole example in the 20s, and the cations were changed over to α -Fe₂O₃ and CaCO₃. The main thrust behind this extraordinary exothermic response was the ignition of NH₄NO₃ delivered in the arrangement balance, and the temperature of the response was 227°C[9-6]. The response speed guaranteed that homogeneity was kept up and gas development made an extremely permeable froth structure that delivered a free agglomeration when powdered. The example was essentially CaM with some α -Fe₂O₃ present after terminating at 700°C. This citrate-burning cycle can be done either by direct burning of a watery gel containing satisfactory groupings of oxidizing specialists (ACS) or by the start of a dried citrate gel powder (LCS)[9,8]. Citrate: metal particle proportion of 60.68 was discovered to be adequate to permit the wet gel to light at 200C for the ACS strategy and to dry the gel for 18 h at 120 °C for ignition to happen at a 1:1:1 proportion (LCS) (LCS) (LCS). This was because higher citrus extract levels consumed more water through hydrogen holding, repressing the response.

Microwave heating can likewise be utilized to actuate burning, where the heat is produced by the collaboration of the microwaves with the materials themselves, commonly at 2.45GHz, the recurrence at which homegrown microwaves work. Single-stage CaM nanopowders (20-50 nm) were acquired by blending a stoichiometric combination of nitrates with citrus extract in ethylene glycol (Acid: Fe=1:5) and ethylenediaminetetraacetic corrosive, adjusted to pH-5-6.5 with alkali arrangement and with an abundance of the measure of ammonium nitrate expected to oxidize all the chelating hydrocarbons. This combination was then freeze-dried and auto-combusted in a microwave with an uncommonly fabricated quartz vessel and sintered ferrite backing to streamline the heating conditions. The immediate arrangement of single-stage nanopowder from the auto burning reaction[100] came about because of this muddled planning.

1.3 M ferrite substituted with M ferrite

The trading of particles was subbed, shaping at 750°C the tainted material. The grains were 9 nm wide and 29 nm thick at 800°C, ascending to 200 nm at 900°C at 130 nm yet keeping up a length to thickness proportion of 1.5 [14]. The development of M ferrites BaFe₁₀Cr₂O₁₉ and SrFe₁₀Cr₂O₁₉ fill in for chromium demonstrated conceivable yet persevered through two distinct systems. α-Fe₂O₃, BaFe₂O₄, and BaCr₂O₄ were shaped as antecedents by heating 5Fe₂O₃, BaCO₃, and Cr₂O₃ together yet the M stage started to frame following 5 minutes at 1020°C. M ferrite was the fundamental stage after 2h, and the barium-containing forerunner stages had vanished, yet a modest quantity of α-Fe₂O₃ stayed at this temperature even after 6 h. Impacts of single-stage BaFe₁₀Cr₂O₁₉ after 1300 °C/2h. The pre-cursor stages with SrCO₃ are α-Fe₂O₃, SrCrO₄, and SrFeO_{3-x}, and SrM had just started to frame at 980°C. Some SrCrO₄ persevered for up to 90min at 980°C, yet after 6 h, the example was practically all M ferrite with follow α-Fe₂O₃. At first, the M stage would in the general frame as unadulterated SrM and the chromium gradually defused into the cross-section to shape SrFe₁₀Cr₂O₁₉ more than a few hours, using the strong arrangement SrFe_{12-x}Cr_xO₁₉[15].

The Al³⁺ particle can likewise be subbed by BaM ferrite up to BaFe_{4.2}Al_{7.8}O₁₉[16], and a full strong arrangement is conceivable among SrM and SrAl₁₂O₁₉[190]. A most extreme substitution of BaFe₅Al₇O₁₉ was accounted for when the citrate gel-auto ignition supportive of cress (at 80°C) was made, and strangely Fe₃O₄ was viewed as an antecedent at 500°C, to be supplanted at 850 °C by α-Fe₂O₃ and M ferrite, likely because of the decrease idea of the burning process[11]. Liu et al. indicated that their aqueous amalgamation of Ba-Fe_{12-x}Al_xO₁₉ could be subbed with x<6, while limited quantities of BaCO₃ and BaFe₂O₄ were seen in the as-orchestrated item with estimations of x > 0.9[161]. The ideal proportion of (Fe + Al): Ba was diminished to 9:5, and until 230°C the M stage was not framed and was not unadulterated until 250°C/4 h responded.

They found that they could utilize higher Fe²⁺ forerunner levels, as Al³⁺ fill in for Fe³⁺, to the point that the antecedent comprised only of Fe²⁺ and Al³⁺ particles for the x= 6 examples, all Fe²⁺ changing over to Fe³⁺ during blend. This was because c-Al₂O₃ is additionally the spinel, and assisted with forming the progression of M. At the point when Al-subbed SrM was created over the entire replacement range, the morphology changed significantly, from hexagonal platelets ~100 nm for SrM to sporadic and rakish particles with up to 4 Al particles and prolonged poles or needles 200 nm long with replacement levels above this[191]. Of the trivalent lanthanides, Ga³⁺ and La³⁺ have the greatest solvency limit, and both lanthanide doped[192] and gallium doped[193] hexaferrite have been delivered with complete iron replacement thinking about the enormous size of the La³⁺ particle.

This demonstrated that the M structure would withstand a specific amount of strong change metal arrangement without imploding, and this was demonstrated right by the creation of a wide scope of doped M ferrites wherein either Me³⁺ or a combination of M²⁺/M⁴⁺ particles are fill in for iron, given that they have similar ionic radii as the subbed particles.

The cross-section boundary, grain size, immersion polarization, coercivity, and remanence are generally de-made with expanding x, however, it was discovered that the Ti⁴⁺ particle affected the grain size while the magnetic properties were changed essentially by the Co²⁺ ion[1-6]. It has been proposed that the grain size is diminished by improving nucleation sites[197] with Ti⁴⁺ particles. The grid boundary is 5.89Å, equivalent to for CaM, however with replacement, the c-hub was found to increment, being 23.20Å at x = 0.8 [198], 23.21 Å at x = 1.1 and 23.23Å at x = 1.5 [199], in light of the fact that the normal span of Co²⁺/Ti⁴⁺ (0.627Å) is more prominent than that of Fe³⁺ (0.550Å).

2. Experimentation

2.1 Synthesis

Calcium-strontium hexaferrite mixes supplanted by aluminum with the Ca_{0.5}Sr_{0.5}Al_xFe_{12-x}O₁₉ synthesis (x=1 and 1.5) were orchestrated utilizing the auto-burning cycle of sol-gel. The technique for amalgamation included the consumption of redox blends in which metal nitrates went about as an oxidizing reactant, while urea went about as the decrease reactant. Ca(NO₃)₂·4H₂O, Fe(NO₃)₃·9H₂O, Sr(NO₃)₂ and Al(NO₃)₃·9H₂O, and CO(NH₂)₂ urea, disintegrated in a glass measuring utensil in 10ml of refined water.

To frame a homogeneous fluid arrangement, the arrangements arranged in the receptacle were blended. On the hot plate after that, the fluid arrangement was warmed. By vanishing the water, following a couple of moments, the fluid arrangement is changed over into wet gel. It starts consuming after the wet gel arrives at the purpose of auto-ignition and turns into a strength that consumes. At the point when all the combustible substances are burned-through, the ignition isn't finished and the subsequent material is a free item displaying voids and pores shaped during the burning response by getting away from gases[17].

The debris of the calcium strontium ferrite fill in for aluminum was gathered after complete ignition. This debris was then ground in a peaceful human for three hours and afterward sintered at a temperature of 800oC for four hours in the stiffler heater and cooled, at that point squashed again for three hours to make a fine calcium strontium hexaferrite aluminum subbed powder.

The hexaferrite is being studied as Sr_{0.5}Ca_{0.5}Fe₁₁AlO₁₉ in Calcium-Strontium. The ions in the simple Ca-Sr compound Fe⁺³ with Al⁺³ can be replaced. In this case, substituted ions were selected to maintain charge neutrality and have to have a deep understanding of the variation of internal properties. In the variations of properties in those ferrites, aluminum plays a dominant role. Using the standard method of sol-gel auto combustion, the recorded samples were synthesized[18].

2.1.1 Al with Sr-Ca Ferrite:

In a polycrystalline state, the composition was sintered by sol-gel auto combustion, by heating the nitrite constituent mixture. The single-phase M-type compound can be obtained via air heating at 800°C. The substitution of Fe⁺³ ions by Al⁺³ ions has been investigated due to the similarity and close structural parameters.

A literature review was conducted by several researchers with a combination of Al^{3+} in calcium strontium hexaferrite and worked on the simultaneous combinational effect of these cations, namely Ca^{2+} and Sr^{3+} , on the electrical, magnetic, and other related properties of M-hexaferrite[8-9]. By arrangement burning strategy, Al subbed nano calcium hexaferrite $CaAl_xFe_{12-x}O_{19}$ ($x = 3, 4$) was blended with metal nitrates as oxidants and ODH as decreasing specialists. Ch., Ch. From Mamatha et al. With rising Al particle focus, the crystallite size and cross-section volume have been appeared to diminish. These materials are made as hard ferrite materials[4] as immersion polarization diminishes with expanding Al particle focus, coercivity, and retentivity increment. Expanded retentiveness and coercivity

$CaAl_xFe_{12-x}O_{19}$ Al nano calcium hexaferrite substitute $CaM_xAl_xFe_{12-x}O_{19}$ ($x = 1,2,3, 4$) was orchestrated by arrangement ignition strategy by ch. Mamatha et al. in 2017 utilizing metal nitrates as oxidants and ODH as lessening specialists. With rising Al particle focus, the crystallite size and cross-section volume have been appeared to diminish.

S.R. Gavali The Al-subbed $CaAl_xFe_{12-x}O_{19}$ nano-calcium hexaferrite ($x = 0, 2, 4$) was combined utilizing urea as fuel by sol-gel auto-ignition. With expanding Al particle fixation, the boundaries of the cross-sections and grid volume have been appeared to diminish. The determined an and c qualities were found to have been 5.8\AA and 22.1\AA respectively [10].

Momentum research has integrated hexaferrite M-type calcium with the recipe $CaAl_xFe_{12-x}O_{19}$ utilizing the sol-gel auto-ignition measure. The predominant sol-gel auto burning technique is demonstrated to be among all strategies. As a quick, clean, and quick cycle, this strategy has the advantages of high homogeneity, high immaculateness, efficient, and superfine powers[11, 12, 13].

In calcium hexaferrite, the replacement of Al particles above focus $x = 1$ is additionally examined, while the grouping of Al particles beneath fixation isn't additionally contemplated. Consequently, an endeavor was made to research and study the underlying and magnetic properties beneath focus 1 of the impact of Al replacement.

Synthetic co-precipitation and micro emulsion-based water-in-oil methods have blended and harmed the hexaferrite particles of $BaCa_2Fe_{16}O_{27}$. From J. R. B. Jotania et al. Sci. Sci. Sci. Sci. A.R. The beginning materials were barium nitrate ($Ba(NO_3)_2 \cdot 6H_2O$), calcium nitrate ($Ca(NO_3)_2 \cdot H_2O$), ferric nitrate ($Fe(NO_3)_3 \cdot 9H_2O$) (> 99.9 percent). Stoichiometric barium nitrate, calcium nitrate, and ferrous nitrate focuses were disintegrated each in turn in 100 ml of de-ionized water. For a pH of -8, the alkali arrangement (30%) was gradually added to the combination.

At room temperature for maturing, the blended arrangement was fomented for two hours and prepared for 24 hours. At 2500 rpm for 20 minutes, the barium-calcium hexaferrite hastens were isolated by an axis machine. The readied encourage washed to eliminate pollutions in a 1:1 combination of methanol and $CH_3)_2CO$ followed by 100% de-ionized water. At 100, the hasten dried out calcinated for 24 hours and $950^\circ C$ to get $BaCa_2Fe_{16}O_{27}$ hexaferrite particles for 4-hours. The cycle was rehashed to get $BaCa_2Fe_{16}O_{27}$ hexaferrite particles within the sight of surfactants for every one of the three surfactants: Cetyl trimethyl ammonium bromide, sodium dodecyl sulfate, polyethylene glycol sorbitan monooleate (0.01M surfactant in 100 ml of deionized water) (0.01M surfactant in 100 ml of deionized water).

Table 3: concentration wise changes in properties[19]

Ca	Sr	Ba	an (Å)	c(Å)	V	Dx	Dm	Mol. Wt.	Porosit y	c/a
0.1	0.	0.7	5.856	23.107	686.4	5.3	4.1	1100.0	22.33	0.2
	2		9	0	5	2	3	9		5
0.1	0.	0.5	5.815	22.783	667.3	5.4	4.0	1090.1	25.85	0.2
	4		7	6	5	2	2	4		5
0.1	0.	0.3	5.817	22.782	667.6	5.3	3.9	1080.2	25.66	0.2
	6		0	3	1	7	9	0		5
0.2	0.	0.5	5.827	22.744	668.9	5.4	3.9	1093.8	27.01	0.2
5	2	5	8	2	7	3	6	0		5
0.2	0.	0.3	5.815	22.763	666.7	5.3	3.8	1083.8	28.13	0.2
5	4	5	8	3	8	9	7	5		5
0.2	0.	0.1	5.807	22.741	664.3	5.3	3.8	1073.9	28.57	0.2
5	6	5	9	0	2	6	3	2		5
0.4	0.	0.4	5.895	23.074	694.6	5.1	3.9	1087.5	23.57	0.2
	2		9	1	3	9	7	2		5
0.4	0.	0.0	5.895	23.136	696.4	5.0	3.8	1067.6	23.88	0.2
	6		6	9	5	9	7	4		5
0.4	0.	0.2	5.895	23.110	695.7	5.1	3.8	1077.5	25.91	0.2
	4		8	8	1	4	1	8		5
0.4	0	0.6	5.902	23.091	696.7	5.2	3.8	1097.4	25.63	0.2
			8	0	6	3	9	7		5

The arrangement strategy for water particles of barium calcium hexaferrite in the oil turn around the micellar procedure has appeared was picked as a surfactant with 4-octylphenol polyethoxylated (Triton X100), n-hexanol as the co-surfactant, cyclohexane as the dissolvable (oil measure), a watery arrangement as the water stage. The fluid cycle was an answer of 0.1 M barium hydroxide, 0.2 M calcium nitrate, and 1.6 M ferric nitrate in microemulsion-I (5ml watery arrangement in 42.5ml microemulsion) (5ml fluid arrangement in 42.5ml microemulsion).

In microemulsion-II, the fluid advance was a smelling salts arrangement (25 %) as the precipitant specialist (5M watery arrangement of alkali in 42.5ml microemulsion) (5M watery arrangement of smelling salts in 42.5ml microemulsion). Dropwise in microemulsion-I was added to get precipitation of barium calcium hexaferrite microemulsion-II under overwhelming mixing for 2 h; at that point, the arrangement was matured for 12 hours. To eliminate the leftover surfactant and natural buildup, the antecedent particles inside the water pool of converse micelles were washed by centrifugation with anhydrous ethanol and water. The hasten was dried in a broiler at 100 °C for 24 hours and afterward calcinated for 4 hours at 950°C, trailed by the cooling of the heater to room temperature.

High-temperature strong state responses of stoichiometric combinations of AR grade CaO, Fe₂O₃, Al₂O₃, and Co₂O₃ oxides were utilized to incorporate polycrystalline CaAl_xCo_xFe_{12-2x}O₁₉ (2 < x < 5) examples. The blend was partitioned into two phases: After calcination noticeable all around for 2 h at 800°C. The blend was ground and dried, packed into pellets, and (ii) at last exposed to transitional crushing warm treatment at 1200°C for 1250 h and

extinguished noticeable all around. The preliminary cycle was indistinguishable from the one recently referenced (Kulkarni and Prakash 1994; Rewatkar et al 1998) (Kulkarni and Prakash 1994; Rewatkar et al 1998)[20].

The stoichiometric measures of AR grade $\text{Ca}(\text{NO}_3)_2 \cdot 4\text{H}_2\text{O}$, $\text{Fe}(\text{NO}_3)_3 \cdot 9\text{H}_2\text{O}$, $\text{Al}(\text{NO}_3)_3 \cdot 9\text{H}_2\text{O}$, and NaOH were utilized as reactants for the planning of tests in the aqueous cycle. Reactants were disintegrated under extraordinary blending in deionized water. The arrangement was filled with a Teflon liner held in an autoclave of treated steel, fixed, and held at 160-C in the broiler. For 18 h, a similar temperature was safeguarded. In the wake of cooling the autoclave in the regular cycle to room temperature, the acquired accelerate was isolated by centrifugation, giving the calcium ferrite, sodium nitrate, and water ionic state. The particles of sodium and nitrate are disengaged by consistently washing with ethanol and deionized water in the arrangement. The arrangement was then dried for 3 hours in a hot-air stove at 80°C[21].

2.2 XRD

The noticed XRD designs are recorded with the JCPDS design M-type hexaferrite standard (document no. 49-1586). The most noteworthy power diffraction pinnacle of the relative multitude of tests was seen at (107) direction. There was a little move in the pinnacle position with an expansion in Al_3^+ + particle fixation. The XRD design comprises of ordinary reflecting planes (006), (107), (202), (109), (206) (214) 303, (332), (222), (224) and (3,0,3) and with (107) direction affirm that the examples arranged have a place with M sort hexaferrite, the most noteworthy force diffraction pinnacles of tests were characterized. With an improvement in aluminum content because of the little ionic range of Al^{3+} ion (0.54Å) over F^{3+} (0.65 Å, for example, top powers, top areas, and pinnacle length, From the area of the most elevated diffraction top, the crystallite size (D) was resolved to utilize the notable Scherrer condition [14].

$$D = \frac{k\lambda}{\beta \cos\theta}$$

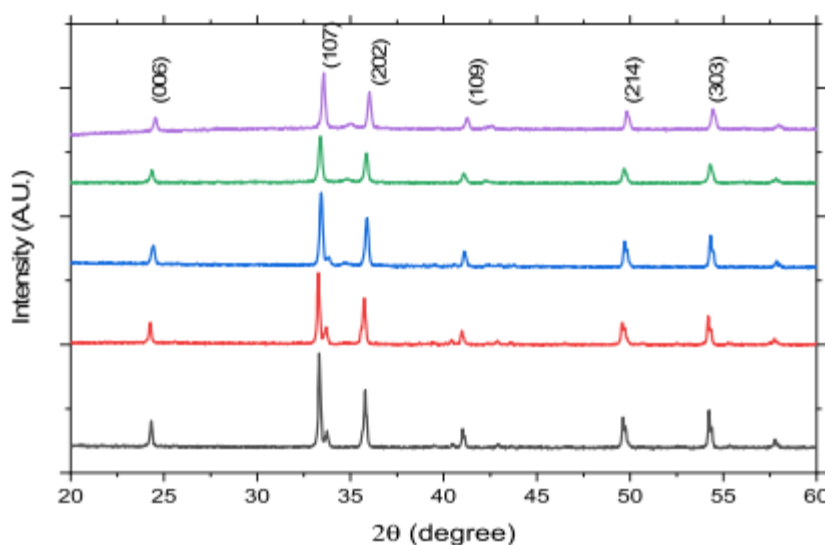


Figure 2: XRD Peaks at different temp and concentration showing the stability

The lattice constants (a and c) and lattice Volume of the unit cell (V_{cell}) were calculated by using the following equations

$$\frac{1}{d^2} = \frac{4}{3} \left(\frac{h^2 + hk^1 + k^2}{a^2} \right) + \frac{l^2}{c^2} \quad (2)$$

$$V_{cell} = \frac{\sqrt{3}}{2} c \cdot a^2 \quad (3)$$

Table 4: The structural properties of the samples with Al substituted Ca Hexaferrite. Fuel urea[19]

Sample	D (nm)	Lattice Parameters		c/a	V (Å)
		a (Å)	c (Å)		
CaFe ₁₂ O ₁₉	74.36	5.87	22.15	3.77	660.9011
CaAl _{0.2} Fe _{11.8} O ₁₉	74.31	5.87	22.19	3.77	663.9358
CaAl _{0.4} Fe _{11.6} O ₁₉	70.03	5.85	22.09	3.77	655.5814
CaAl _{0.6} Fe _{11.4} O ₁₉	68.41	5.85	22.11	3.77	657.3745
CaAl _{0.8} Fe _{11.2} O ₁₉	62.12	5.83	22.00	3.77	648.0615

It was seen that with an expansion in Al particle fixation, the grid boundaries (an and c), cross-section length, and crystallite size diminished. Run of the mill room-temperature hysteresis circles for Ca Al_xFe_{12-x}O₁₉ tests (x = 0, 0.2, 0.4, 0.6, 0.8) arranged utilizing the sol-gel auto-ignition technique are appeared in the nanoscope of the crystallite sizes for all examples.

Ch Mamatha: Ca Al_xFe_{12-x}O₁₉ All pinnacles consummately suit Bragg Hexagonal structure reflection with space bunch P6/MMC and PCPDF NO. 49-1586. A nearby investigation of the PXRD design uncovers that the boundaries contrast somewhat.

There are five F³⁺ positions in the magnetoplumbite precious stone grid, which are 2a, 2b, 12k, 4f, and 4f. 4f is the tetrahedral site of these grid destinations, 2b is the bi-pyramidal site, and 2a, 12k, and 4f are octahedral locales. The precious stone grid shrinkage[19-22] is brought about by Al³⁺ F³⁺ replacements. Subsequently, the deviation of the precious stone grid causes the boundaries a, c, and contrast in the sweep of the gem grains to change in the gem cross-section. This variety in the size of the crystallite prompts a diminishing in the thickness of X-beams and is answerable for the move in pinnacles of X-beam diffraction. The c/a proportion is inside the normal scope of 3.94 to 3.96 and demonstrated the improvement of a hexagonal structure of the M-type[23]. The proportion of cross-section boundaries c/a

might be utilized to quantify the kind of structure and the hexaferrite structure of the M-type can be thought of if the proportion of grid boundaries is lower than 3.98.

Table 5: XRD Analysis of the compound with fule as urea in combustion synthesis[23]

Compound	D (nm)	a(A°)	c (A°)	V(A ³)	c/a
CaFe ₁₂ O ₁₉	33	6.049	22.051	699.48	3.644
CaAlFe ₁₂ O ₁₉	30	6.010	22.033	689.831	3.665
CaAl ₂ Fe ₁₂ O ₁₉	32	6.004	22.006	687.572	3.665
CaAl ₃ Fe ₁₂ O ₁₉	31	5.998	21.934	684.080	3.656
CaAl ₄ Fe ₁₂ O ₁₉	24	5.985	21.917	680.611	3.661

The preparation of the chemical formula polycrystalline compounds with and was performed (using the normal ceramic process. It was chosen to remain unchanged for the molecular concentration by the stoichiometry of the compound and substituted cations. As the starting precursors for the synthesis of the compound sequence, the AR grade oxides Fe₂O₃, La₂O₃, Ca₂O₃ The preparation method consisted of mixing oxides with the appropriate stoichiometry and grounding them in an agate mortar together in an acetone medium. The synthesis was organized into two phases. The mixture was initially calcinated for 8h in the air at 773K, followed by further mixing and extensive grinding, and final thermal treatment for 72h at 1430K.

Table 6: Glycine combustion process[23]

Compound	D (nm)	an (A°)	c (A°)	V(A ³)	c/a
CaFe ₁₂ O ₁₉	33.43	5.809	22.342	652.48	3.844
CaFe ₁₂ O ₁₉	30.47	5.803	22.287	649.931	3.85
CaFe ₁₂ O ₁₉	32.59	5.805	22.253	649.372	3.85
CaFe ₁₂ O ₁₉	30.8	5.986	21.823	677.180	3.646
CaFe ₁₂ O ₁₉	23.4	5.975	21.949	679.511	3.671

Table 7: hydrothermal synthesis method with glycine fuel[23]

Compound	D (nm)	an (A°)	c (A°)	V(A ³)	c/a
CaFe ₁₂ O ₁₉	41.38	5.998	22.856	712.08	3.81

CaFe ₁₂ O ₁₉	37.61	5.995	22.851	711.22	3.81
CaFe ₁₂ O ₁₉	19.53	5.993	22.844	710.52	3.81
CaFe ₁₂ O ₁₉	13.36	5.806	22.394	653.74	3.86
CaFe ₁₂ O ₁₉	38.2	5.816	22.368	655.23	3.85

The estimations of the grid boundaries fluctuate somewhere in the range of 5,8079 and 5,9208 Å, yet additionally somewhere in the range of 22.7442 and 23.2143Å. the XRD profiles of the standard M-hexaferrite appear alongside the noticed X-beam diffraction examples of the multitude of tests. The presence of reflection planes (006), (107), (114), (201), (108), (220) and (304) comparing to the unadulterated hexaferrite magnetoplumbite stage having a place with the P63/MMC space bunch has likewise been recognized (No. 194)[14].

As the qualities exist in the unadulterated magnetoplumbite stage cross-section boundary scope of hexaferrite (= 5.8–5.9 Å and = 22–23Å), the outcomes are likewise confirmed by the expressed grid boundary esteems. Since La³⁺ particle (1.13Å) has ionic radii lower than Sr²⁺ (1.27Å) particle, notwithstanding, replacement of La³⁺ for Sr²⁺ particle seems to prompt diminishing grid boundaries.' Thus, for the example with the most minimal measure of La³⁺ particle, the cross-section extension was finished up to be more noteworthy.

While the normal ionic sweep of subbed cations can be brought about by varieties in the general grid boundary, the proportion has remained genuinely consistent. In La³⁺ subbed M-type strontium ferrites[15–17], comparable action has been accounted for. Regarding pieces or test codes, the distinction between electric conductivity and dielectric steady is (R-1 to R-10). An expansion is seen notwithstanding the expanding replacement of Sr²⁺ and La³⁺ particles with compound R-7, which is trailed by a diminishing to R-10. For electrical conductivity and dielectric consistent, the most extreme worth is gotten for test R7, with a proportion of Ca²⁺ = 0.4, Sr²⁺ = 0.2, Ba²⁺ = 0.4, and La³⁺ = 0.3.

The little polaron jumping cycle and Maxwell Wagner interfacial polarization can explain these discoveries. The two components manage Fe²⁺ particle creation coming about because of the incomplete substitution of Fe²⁺, Fe³⁺ at octahedral site 4f1 or 2b and volatilization during the sintering cycle of subbed particles. It very well may be dealt with independently in the tetrahedral site and octahedral site encompassed by oxygen particles (barring just three-sided bipyramidal site) detached from one another as the structure with cations and anions. Subsequently, the confined electron model is more reasonable for tending to the condition component instead of the band model, in particular the bouncing instrument.

The semiconducting marvel is required to overwhelm the Sr²⁺ La³⁺ particle collaboration and solvency until R7, to make up for charge impartiality at the 4f1 or 2b site, and to produce electron move somewhere in the range of Fe²⁺ and Fe³⁺ [27]. In compound R-7, the high electrical conductivity esteem additionally mirrors the exchange of the most extreme number

of Fe^{2+} particles engaged with the trade collaboration wonder somewhere in the range of Fe^{2+} and Fe^{3+} , prompting the greatest conduction stage. Among the mixes with high La^{3+} particle focus, this could be because of high initiation energy ($=0.31\text{eV}$) alongside Ba^{2+} and Sr^{2+} . As demonstrated, the progress energy somewhere in the range of Fe^{2+} and Fe^{3+} is 0.2eV , and if the actuation energy of the resistivity is more prominent than 0.28eV , the energy is essentially utilized not to produce extra charging transporters yet to move charges[26]. Higher La^{3+} particle fixation at the grain limits adds to high charge portability and a decline in Fe^{3+} particle focus, which builds conductivity steadily and reflects semiconducting behavior[28, 29].

The result of the writing survey shows that 12k, 2a, and 4f1[19, 24] positions are wanted to involve the subbed Al^{3+} particles. Al^{3+} particles enter the 4f1 site ($x = 0.0$ to $x = 0.6$) for a lower Al^{3+} particle fixation. Site 4f1 has an electronic design turn down. This drops the turn down electronic design of the electrons and expands the upward turn direction of the electrons. An improvement in the subsequent magnetic second and charge of immersion is the impact. Al^{3+} particles join the 12K site for higher Al^{3+} particle focuses (above $x = 0.6$).[20] The turn-up electronic arrangement of the 12K site. The turn down electronic design in the upward turn course builds the electrons and diminishes the electrons. By expanding the substitution of Al^{3+} particles ($x > 0.6$) rather than Fe^{3+} particles, the $\text{Fe}^{3+}\text{-O-Fe}^{3+}$ super-trade collaboration is likewise diminished. The total impact is that as a result, the magnetic second and immersion polarization decline.

2.3 Compositional Magnetic Parameter Variation

In M sort mixes, the area of the magnetic snapshot of the ferric particles in the precious stone is commonly antiparallel to one another along the c-hub. L. Neel (1948) and Anderson (1950) first considered, from a hypothetical perspective, that these magnetic particle arrangements can be acknowledged by supershift cooperation through oxygen particles, which has likewise been exhibited by trial evidence. For these trade connections [13-14], turn synchronization is dependable. The cooperation between two related areas, for example, 2a-12k, 2a-4f¹, and 4f¹-12k are basic for a decent magnetic character in magnetoplumbite. In this way, if the non-magnetic Al^{3+} particles supplant Fe^{3+} particles in the 12-k sublattice, the debilitating of the super-trade communication between magnetic particles brings about a genuinely slanted paramagnetic nature. At 2a and 12k destinations, the presence of Al^{3+} ions in the grid demonstrates a lessening in connection energy, and a reduction in the temperature of the Curie was seen in the compound.

Considering these outcomes, we can presume that the most extreme incentive for magnetic immersion was appeared in the example (Ms with arrangement Ca = 0.1, Sr = 0.6, Ba = 0.3, and La = 0.1 with creation Ca = 0.1, Sr = 0.6, Ba = 0.3, and La = 01) (Ms). In contrast with Ba^{2+} in the replacement, the noticed expansion in magnetic second immersion, retentivity, and coercivity exhibited high solvency and collaboration somewhere in the range of La^{3+} and Sr^{2+} . The charge esteem increment mirrors the octahedral substitution of particles at the turn-down-sublattice site[28-29].

The deficiency of magnetocrystalline anisotropy and the formation of huge scope magnetic particulate anisotropy[33] may clarify the ascent in coercivity. The replacement of nonmagnetic particle La^+ increments, nonetheless, for additional examples with consistent Sr^{2+} content, recommending an abatement in magnetic boundaries. This qualification in the marvel known as the inclining turn structure assumes its job when an adjustment in valency from one Fe^{3+} to Fe^{2+} is related to the replacement of trivalent particles for divalent particles, which diminishes the association power.

This outcome in the progress of the magnetically troublesome pivot, for example, the C-hub in the turn structure, from collinear to non-collinear. This exhibited huge help for our discoveries and prompted the support of the assumption that all M-hexaferrite could be overwhelmed by the trading of Fe^{3+} to Fe^{2+} alluding to octahedral locales and Fe^{2+} anisotropy on the octahedral site[20-25].

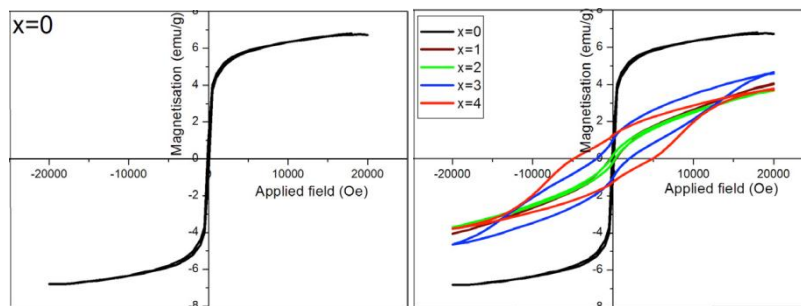


Figure 3: Magnetic property variation with doping concentration

Hysteresis of calcium ferrite without replacement. Figure 3 shows the difference between hysteresis and aluminum substitution, and Figure 4 shows the correlation. The state of the curves implies that examples are ferrimagnetic. The field of the ring displays the idea of the hard magnetic property. The ascent in magnetocrystalline anisotropy is inferable from increments in coercivity noticed.

At room temperature, a field-subordinate charge of the diverse Ba-Ca hexaferrite powders was estimated on a vibrating test magnetometer with a most extreme field of 15kOe applied. The examples' underlying bends of charge and circles of hysteresis have appeared in Figs. 5a, 5b, and 5c individually, separately. It was demonstrated that the example arranged within the sight of sodium dodecyl sulfate showed higher immersion (M_s) polarization, lingering charge (M_r and inborn coercivity (H_c) than different examples. The M_r/M_s esteems are around 0.5 for all the examples, demonstrating that $\text{BaCa}_2\text{Fe}_{16}\text{O}_{27}$ powder was created from single magnetic domains[32]. Table: Magnetic attributes.

Table 8: An Al-focus magnetic property[30]

compound	M_s (emu/gm)	H_c (Oe)	M_r (emu/gm)	M_r/M_s
$\text{CaFe}_{12}\text{O}_{19}$	0.49	3493.10	0.13	0.26

Ca Al _{0.2} Fe _{11.8} O ₁₉	0.69	1343.40	0.11	0.10
Ca Al _{0.4} Fe _{11.6} O ₁₉	1.02	834.50	0.14	0.13
Ca Al _{0.6} Fe _{11.4} O ₁₉	2.10	138.28	0.10	0.05
Ca Al _{0.8} Fe _{11.2} O ₁₉	2.08	235.10	0.12	0.06

Magnetic properties, for example, immersion magnetization (Ms), remaining magnetization (Mr), coercive power (Hc), equilibrium proportion (Mr/Ms and magnet second per Bohr magneton recipe unit. Coercivity esteems increment with replacements for A³⁺. This is a decent increment when contrasted with the recently recorded estimation of 21.130e for CaFRe₈Al₄O₁₉[24]. Coercivity from each of the five examples of To is discovered to be more suitable for CaFe₁₀Al₂O₁₉.

Mr. Estimations of Mm, viz, affirms the presence of three kinds of space states. Superparamagnetic (SD) multi-area (MD) and single space [25-27]. With the help of the equilibrium proportion, magnetocrystalline anisotropy and exchange relations can be approximately broke down. The parity proportion, which is the proportion of Mr. remanent charge to Ms. charge immersion at or above 0.5, has been accounted for to mean the proportion of Mr. charge immersion at or above 0.5

The production of the multi-space structure can be because of the material inside the single magnetic area and underneath 0.5. It is clear from the deliberate qualities that all examples have a structure with numerous spaces. When all is said in done, if it happens beneath 0.5, the ferrite SQR esteem is fine for the vehicle of recording[22]

2.4 Electro-electric

Compositional Variation of Electric Conductivity and Dielectric Constant. Both are electrical properties, electrical conductivity, and dielectric consistency, and it has been perceived that the distinction in the two properties is answerable for this cycle, specifically, electron trade among Fe²⁺ and Fe³⁺. Electrical conductivity and the steady dielectric contrast in example code structure (R-1 to R-10). An ascent is seen notwithstanding the expanding replacement of Sr²⁺ and La³⁺ particles for compound R-7, which is additionally trailed by a decline. The most extreme incentive for the extent of Ca²⁺ = 0.4, Sr²⁺ = 0.2, Ba²⁺ = 0.4 and La=0.3 is acquired for electrical conductivity and the dielectric steady.

These discoveries can be clarified by the little polaron bouncing cycle and Maxwell Wagner interfacial polarization. The two components manage the development of Fe²⁺ Fe³⁺ particles because of the fractional substitution of Fe³⁺ at octahedral site 4f 1 or 2b and the volatilization of the substitution particles during the sintering cycle. As the structure with cations and anions independently in the tetrahedral site and octahedral site encompassed by oxygen particles (barring just three-sided bipyramidal site) separated from one another can be dealt with. In this way, the restricted electron model, to be specific the jumping system, is

more appropriate for tending to the condition instrument instead of the band model. To rule the semiconducting wonder, Sr^{2+} La^{3+} particle communication and dissolvability are important to make up for charge impartiality at the site of $4f^{2+}$ 1 or $2b$ and create electron move among Fe and Fe^{3+} [27].

The high electrical conductivity esteem in compound $2+$ additionally mirrors the exchange of the most extreme number of Fe particles engaged with the wonder of trade contact between Fe, prompting the greatest period of conductivity. It very well might be because of the high actuation of energy (E_A^{2+} and $Fe = 0.31eV$) among mixes with a high grouping of La^{3+} particles along with Ba^{3+} .

Calcium ferrite hysteresis without substitution. The distinction between hysteresis and aluminum substitution appears in figure 3 and the connection appears in figure 4. Tests are ferrimagnetic as a result of the type of curves. The embodiment of the hard magnetic property shows the field of the ring. The expansion in magneto-crystalline anisotropy is because of expansions in noticed coercivity.

The field-subordinate magnetization of the different Ba-Ca hexaferrite powders was estimated at room temperature on a vibrating test magnetometer with a most extreme field of 15kOe applied. The examples' underlying charge bends and hysteresis circles appear in 5a, 5b, and 5 c separately. Table records the magnetic boundaries. The example arranged within the sight of sodium dodecyl sulfate was appeared to show higher immersion (M_s) polarization, remaining charge (M_r and natural coercivity (H_c) than different examples. For all the examples, the M_r/M_s esteems are about 0.5, recommending that $BaCa_2Fe_{16}O_{27}$ powder was gotten from single magnetic domains[32]. Table: Magnetic highlights.

Table 8: A magnetic property with Al-focus[33]

Ca	Sr	Ba	a(Å)	c(Å)	$E_A(ev)$	Rho Dc(ohm m)	Rho ac(ohm m m)	M_s	Mr	Hc	Tc
0.1	0.2	0.7	5.8569	23.1070	0.34	0.0553	2.5	49.298	24.339	2307.5	700-750
0.1	0.4	0.5	5.8157	22.7836	0.31	0.0444	1.11	57.88	30.440	2427.3	700-750
0.1	0.6	0.3	5.8170	22.7823	0.35	0.0720	1.49	68.471	35.569	2904.6	700-750
0.25	0.2	0.55	5.8278	22.7442	0.279	0.328	3.89	55.610	23.671	1170.8	670-690
0.25	0.4	0.35	5.8158	22.7633	0.265	0.444	2.59	48.143	23.043	2074.8	670-700
0.25	0.6	0.15	5.8079	22.7410	0.268	0.708	4.48	52.98	23.297	2327.14	670-700
0.4	0.2	0.4	5.8959	23.0741	0.31	0.737	6.58	54.811	22.200	1074.9	650-670
0.4	0.6	0.0	5.8956	23.1369	0.248	0.647	7.54	54.140	26.934	2101.8	650-670

0.4	0.4	0.2	5.8958	23.1108	0.244	0.3286	5.31	43.381	19.910	1671.1	650-670
0.4	0	0.6	5.9028	23.0910	0.265	0.1369	4.76	52.350	21.670	1091.1	660-670

The chart shows magnetic properties, for example, the magnetization of immersion (Ms), lingering magnetization (Mr), coercive power (Hc), equilibrium proportion (Mr/Ms and magnet second per Bohr magneton. Estimations of coercivity increment with A³⁺ replacements. When contrasted with the recently announced estimation of 21.13Oe for CaFe₈Al₄O₁₉[24], this is a solid increment. Coercivity is discovered to be more fit to CaFe₁₀Al₂O₁₉ from each of the five.

2.5 Temperature Curie's

It is noticed that the Curie temperature Tc (K) was higher in the example with a lower measure of La³⁺ particle. This pattern might be ascribed to the associations between different magnetic particles, the grouping of these particles, and their magnetic force. In this manner, a higher measure of energy is thought to be expected to beat the impacts of trade associations in a substance with a higher number of magnetic particles. Contrasted with the magnetic snapshot of 10μB[34], since the magnetic snapshot of the La³⁺ particle is 2.78μB for the two Fe³⁺ particles, this reasons that the substitution of Fe³⁺ particles by lower La³⁺ and Sr²⁺ particles is probably going to expand the hard magnetic properties and Curie temperature.

In any case, lower esteems for different examples can be clarified dependent on the number of magnetic particles present in the two sublattices and their complementary constriction. The quantity of magnetic particles at the two locales starts to diminish as Fe³⁺ particles are continuously supplanted by uncommon earth La³⁺ particles, prompting a lessening in the communication of Fe³⁺-O²⁻Fe³⁺ type exchange[33]. As the Curie temperature, Tc(K) is controlled by the all-out strength of the trade collaborations, the debilitating of trade associations bring about a decline in the Curie temperature[29], which is in acceptable concurrence with our result.

The magnetic second was accounted for to research the magnetic properties of incorporated examples as a component of the polarizing field at room temperature going from -20kG to +20 kG with the guide of the vibration test.

Vibrating magnetometer (VSM) The decided immersion magnetization (Ms), Coercivity (HcO2), and maintenance esteem appear in Table. An abatement in immersion magnetization(M) with an expansion in Al levels is demonstrated by the after-effects of the VSM considers. Expanded magnetic properties, for example, Coercivity (Hc) and Retentivity (R), have affirmed the presence of hard ferrites (M)1, 27, 30].

Table 10: A magnetic fixed-fixation property[30]

Compound (MΩ/cm)	Hc (Koe)	Ms (emu/g)	Mr (emu/g)	Resistivity At RT ρ	Activation energy
------------------	----------	------------	------------	---------------------	-------------------

					$\Delta E(\text{eV})$	
					Feri	Para
$\text{CaAl}_3\text{Fe}_9\text{O}_{19}$	2.017	3.874	0.869	17.017	0.09	0.98
$\text{CaAl}_4\text{Fe}_8\text{O}_{19}$	5.092	3.791	1.278	28.189	0.18	1.2

the magnetic properties of blended mixes, the magnetic second was recorded as a magnetic second. The polarization fieldwork goes from -20 kG to +20 kG at room temperature. With an expansion in Al fixation, estimated saturation magnetization(Ms), Coercivity(Hc), and Retention(Mr) values, VSM considers showing a decrease in saturation polarization (Ms). The presence of hard ferrites has been exhibited by expanded magnetic properties, including coercivity (Hc) and maintenance (Mr). A consistent ascent in dc electrical resistivity with an expansion in Al content at room temperature was seen in the initiation energy of the examples[33-34].

3. Conclusion

The primary investigation of the examples uncovers that when contrasted with Sr^{2+} and Fe particles, Ca^{2+} doesn't substitute Ba^{2+} in appropriate amounts. A move of valance from Fe^{2+} to Fe^{3+} at the octahedral 2a or $4f^2$ position corresponds with the replacement of La^{3+} for Ba^{2+} and Sr^{2+} in M-type hexaferrite. Among the examples with a higher Sr^{2+} fixation with a fitting La^{3+} focus in M-hexaferrite, there is the best distinction in AC. Alongside conduction, conductivity, and dielectric polarization permit us to gather the development of abundance Fe^{2+} particles and to be upheld dually by the thermoelectric strength negative worth. Because of quite a raised dielectric boundary esteem, it tends to be favorable for such RAMs to be tended to for use. High magnetic boundary esteems for La-subbed Ca, Sr, Ba, and M-hexaferrite (R3) were likewise seen in magnetic investigations to manage high collaborations somewhere in the range of La^{3+} and Sr^{2+} particles and encourage the development of single-area particles as turn revolution happens in the polarization stage rather than space divider relocation. It is conceivable to choose such examples for the making of perpetual magnets.

Utilizing reverse micellar and substance co-precipitation strategies, barium calcium hexaferrite ($\text{BaCa}_2\text{Fe}_{16}\text{O}_{27}$) particles were incorporated. The sort of surfactant and the cycle of readiness have been found to assume a vital function in deciding the morphology and charge of the particles. With the doping of Al^{3+} and Mn^{3+} , calcium ferrite dependability is sufficient and it will increment, and the Ba doped ferrite likewise has more grounded magnetic properties. The doped uncommon earth material shows a more noteworthy impact over the magnet's electrical guideline and morphological control.

Acknowledgment

The author Jay Singh would express the thankfulness toward CSIR –JRF for providing financial support for this work. (File no 09/935(0006)/2019-EMR-I)

Conflict of interest

None of the authors has any conflict of interest with the data published previously and the authors declare no conflict of interest. In the financial term

Reference

1. K.G. Rewatkar, N.M. Patil, S.R. Gawali, Synthesis and magnetic study of Co-Al substituted calcium hexaferrite, *Bull. Mater. Sci.* 28 (6) (2005) 585–587.
2. Robert C. Pullar, Hexagonal ferrites: A review of the synthesis, properties, and applications of hexaferrite ceramics, *Progress in Materials Science* 57 (2012) 1191–1334
3. R.B. Jotania, R.B. Khomane, C.C. Chauhan, S.K. Menon, B.D. Kulkarni, Synthesis and magnetic properties of barium–calcium hexaferrite particles prepared by sol-gel and microemulsion techniques, *J. Magn. Magn. Mater.* 320 (2008) 1095–1101.
4. Y. Yang, J. Shao, F. Wang, D. Huang, Effect of Al doping on the magnetic properties of Sr_{0.1}Ca_{0.6}La_{0.3}Al_xFe_{12-x}O hexaferrite magnets, *J. Ceram. Process. Res.* 18 (7)(2017) 501–505.
5. K.G. Rewatkar, G.S. Prakash, D.K. Kulkarni, Synthesis and characterization of the CaFeXAl_x(CuTi)_{6-x}O hexaferrite system, *Mater. Lett.* 28 (4–6) (1996) 365–368.
6. K. Mehmood, X. Liu, Y. Yang, S. Feng, J. Tang, Z. Ali, Z. Wazir, M.W. Khan, M. Shezad, M.S. Iqbal, C. Zhang, C. Liu, Structural, morphological and magnetic properties of Sr_{0.3}La_{0.48}Ca_{0.25}n [Fe_(2-0.4/n)O₃]Co_(n/45.5, 5.6, 5.7, 5.8, 5.9, 6.0)hexaferrite prepared by 7. facile ceramic route methodology, *J. Magn. Magn. Mater.* 449 (1) (2018) 360–365
7. B.S. Satone, K.G. Rewatkar, S.B. Satone, Structural, electrical and magnetic properties of La/Al substituted nano calcium hexaferrite prepared by sol-gel auto combustion method, *Int. J. Sci. Res.* 6 (2) (2017) 2125–2131.
8. [12] M.S. Hossain, Y. Aktery, et al., Influence of Ni substitution on structural, morphological, dielectric, magnetic and optical properties of Cu–Zn ferrite by double sintering sol-gel technique, *J. Adv. Dielectr.* 9 (2) (2019) 195-0020.
9. Ch. Mamatha, M. Krishnaiah, C.S. Prakash, Effect of synthesis method on the particle size of aluminum-doped hexaferrite, *Int. J. Adv. Sci. Tech. Res.* 5 (5) (2015) 42–46.
10. P. Shepherd, K.K. Mallick, R.J. Green, Magnetic and structural properties of M-type barium hexaferrite prepared by co-precipitation, *J. Magn. Magn. Mater.* 311 (2) (2017) 683–692.
11. A.H. Najafabadi, R. Mozaffarinia, A. Ghasemi, Microstructural characteristics and magnetic properties of Al-substituted barium hexaferrite nanoparticles synthesized by auto-combustion sol-gel processing, *J. Supercond. Nov. Magn.* 2(3),(2015),210-219.
12. V.S. Shinde S.G. Dahotre, L.N. Singh, Synthesis and characterization of aluminum substituted calcium hexaferrite, *Heliyon*, 6 (2020),1022-1025
13. K.G. Rewatkaar, S. V. Gavaali Synthesis and magnetic study of Co–Al substituted calcium hexaferrite *Bull. Mater. Sci.*, 28(6), 2005, 585–587.
14. Almessiere MA, Slimani Y, El Sayed HS, Investigation of Microstructural and magnetic properties of BaV_xFe_{12-x}O₁₉ Nano hexaferrites. *J Supercond.*;32, (2019),1437–1445.
15. Jayakumar K, Dinesh A, Manikandan A, et al. Structural, morphological, enhanced magnetic properties, and antibacterial bio-medical activity of rare earth element (REE) cerium (Ce³⁺) doped CoFe₂O₄ nanoparticles. *J Magn Magn Mater.*;476(2019),157–165.

16. Almessiere MA, Slimani Y, Baykal A. Structural and magnetic properties of Ce-doped strontium hexaferrite. *Ceram Int*;44(2018),9000–9008.
17. Almessiere MA, Slimani Y, Tashkandi NA, et al. The effect of Nb substitution on magnetic properties of BaFe₁₂O₁₉ nano-hexaferrites. *Ceram Int*;45(2019), 1691–1697.
18. Slimani Y, Güngüneş H, Nawaz M, et al. Magneto-optical and microstructural properties of spinel cubic copper ferrites with Li-Al co-substitution. *Ceram Int*;44(2018),14242–14250
19. M.ME. Barakat, D. El-Said Bakeer Structural, Magnetic Properties and Electron Paramagnetic Resonance for BaFe_{12-x}Hg_xO₁₉ Hexaferrite Nanoparticles Prepared by Co-Precipitation Method, *Journal of Taibah University for Science*, 14(1), (2020) 640–652,
20. Ch. Mamatha, M. Krishnaiah, and B. Sreedhar, Enhancement of magnetic properties of calcium Hexa ferrites with aluminum substitution, *Procedia Eng.* 2(1) 5, (2017), 130.
21. MouhsineLaayati, Omar Mounkachi, Larbi El Firdoussi, Mustapha Ait Ali, LahcenFkhar, M-Type SrFe₁₂O Ferrite: An Efficient Catalyst for the Synthesis of Amino Alcohols under Solvent-Free Conditions, *Hindawi Journal of Chemistry* (2020), 10
22. J. N. Christy K. G. Rewatkar *Structural and Dielectric Properties of Substituted Calcium Hexaferrites (IJERT)* **8(7),(2019)**
23. T. Baskaran, A. Joshi, G. Kamalakar, and A. Sakthivel, “A solvent-free method for preparation of β-amino alcohols by ring-opening of epoxides with amines using MCM-22 as a catalyst,” *Applied Catalysis A: General*, 524, (2016) 50–55,
24. N. Azizi, P. Kamrani, and M. Saadat, “A magnetic nano-particle-catalyzed regioselective ring-opening of epoxides by aromatic amines,” *Applied Organometallic Chemistry*, 30(6) (2016), 431–434,
25. A. Sheoran, M. Dhiman, S. Bhukal, et al., “Development of magnetically retrievable spinel nano ferrites as efficient catalysts for aminolysis of epoxides with amines,” *Materials Chemistry and Physics*, vol. 222, pp. 207–216, 2019.
26. MouhsineLaayati, Omar Mounkachi, and Larbi El Firdoussi Ali Hasnaoui, NayadAbdallah, Soufiane El Houssame SaadiaOubaassine, Mustapha Ait Ali, M-Type SrFe₁₂O Ferrite: An efficient Catalyst for the Synthesis of Amino Alcohols under Solvent-Free Conditions, *Hindawi, Journal of Chemistry*,5(3)2020,
27. Suresh S Darokar, Structural and Magnetic Properties of Al Ion Doped Ca-Sr Ceramics Synthesized by Sol-Gel Auto-Combustion Technique 3+, *International Journal of Science and Research (IJSR)*, 9 (4), (2020), 513-517.
28. Studies On Structural, Electric, Dielectric And Magnetic Properties Of Nickel-Based Ferrite Materials, Arba minch, Ethiop MSc Thesis Selamu Shamebo, February 2018
29. Kesavamoorthi R., Vigneshwaran A.N., Sanyal V., and Raja C.R. Synthesis and characterization of nickel ferrite nanoparticles by sol-gel auto combustion method. *Journal of Chemical & Pharmaceutical Sciences*, 9, (2016)160-161
30. Babu K.V., Chandra M.R., Kumar G.V.S., Jagadeesh K. Effect of cobalt substitution on structural, electrical, and magnetic properties of NiFe₂O₄, *Processing and Application of Ceramics*, 11, (2017), 60–66.
31. Khangembam S., Victory M., Surchandra W., Phanjobam S. Electrical and structural properties of zinc substituted nickel ferrites synthesized by sol-gel technique. *Advanced Materials Proceedings*, 2(3), (2017), 162-166.
32. Ghosh, S., Patel, P.C., Gangopadhyay, Structural and Magnetic Studies of Thermally Treated NiFe₂O Nanoparticles. *Metallic and Mate Trans A*,48, (2017). 6135.

33. Lakshmi, M., Kumar V.K. and Thyagarajan, K. Structural and Magnetic Properties of Cr-Co Nanoferrite Particles. *Advances in Nanoparticles*, 5, (2016). 103-113.
34. Suresh, Shinde S. Experimental Techniques to Study Physical, Electric, Dielectric, and Magnetic Properties of Ferrites: A Survey. *International Advanced Research Journal in Science, Engineering and Technology*, 4(5), (2017). 4- 5.